Available online at www.sciencedirect.com

ScienceDirect

Procedia Earth and Planetary Science 9 (2014) 64 – 73

Procedia
Earth and Planetary Science

The Third Italian Workshop on Landslides

Mathematical modelling of slopes

E.E. Alonso[a,*] N.M. Pinyol[a,b] & A. Yerro[a]

[a]*Department of Geotechnical Engineering & Geosciences, UPC, Barcelona, Spain*
[b]*International Center for Numerical Methods in Engineering*

Abstract

The paper discusses first the effect of rainfall on the stability of slopes and it focusses on the role of permeability. Existing or induced discontinuities are shown to have a remarkable effect on the slope safety. Also, the relevance of changes in hydraulic properties in weathered profiles is discussed through a real case. The performance of modern "Lagrangian particle" methods and their capabilities to deal with large displacements is presented. The cases solved refer to brittle materials, a common situation in overconsolidated high plasticity clays.

Selection and peer-review under responsibility of Dipartimento di Ingegneria Civile, Design, Edilizia e Ambiente, Seconda Università di Napoli.

Keywords: landslides, models, rainfall, permeability, unsaturated soils, Material Point Method, brittle soils, run-out, progressive failure.

1. Introduction

Two main topics are covered in this paper: Slopes in partially saturated soils and the modelling of large deformations. Unsaturated slopes may become unstable under the action of rainfall. Two scenarios are analyzed: the effect of development of shearing zones of high permeability and the response of heterogeneous profiles, which are a common circumstance in weathered profiles.

The second topic concerns large deformations and displacements. New computational procedures that combine finite element techniques and Lagrangian integration points are capable of handling large displacements in a dynamic formulation of equilibrium equations. The procedure will be illustrated through some examples.

* Corresponding author. Tel.: +34 934016862; fax: +34 934017251.
E-mail address: eduardo.alonso@upc.edu

Selection and peer-review under responsibility of Dipartimento di Ingegneria Civile, Design, Edilizia e Ambiente, Seconda Università di Napoli.
doi:10.1016/j.proeps.2014.06.002

2. Slopes in unsaturated soils. Rain effects

2.1. Modelling permeability in tensile strain-induced discontinuities

Tensile straining will result in open discontinuities. Shearing of overconsolidated soils implies dilatancy effects, which may produce also the opening of discontinuities. Shearing bands in landslides have also been recognized as preferential paths for flow. If compared with a porous media, a discontinuity characterized by a given aperture, b, results in a significant increase in equivalent permeability. If a Poiseuille type of flow is assumed to occur in the discontinuity, it is easy to show that the equivalent intrinsic permeability of the combined porous media and discontinuity is given by

$$k = \frac{b^3}{12s} + k_{porous} \tag{1}$$

where k_{porous} is the permeability of the matrix and s is a reference distance (s may be identified as the spacing between pre-existing discontinuities in a shale rock, for instance).

Olivella & Alonso[1] described a simple but powerful procedure of introducing this idea into a continuous finite element analysis when discussing the flow of gas through soils. However, the idea is also well suited to analyze the water flow. The procedure is illustrated in Figure 1. If in a given element, a tensile strain, $\Delta\varepsilon$, is calculated at a given step of the analysis, a planar opening of aperture

$$b = b_0 + \Delta b = b_0 + s\Delta\varepsilon \tag{2}$$

is assumed to develop. b_0 is the initial aperture. The discontinuity modifies the equivalent permeability of the element following Equation (1) and it also modifies its water retention. In fact, the air entry value "P" of the element is shown to scale with the cubic root of permeability.

$$P = P_0 \sqrt[3]{\frac{k}{k_0}} \tag{3}$$

where k_0 is the original permeability of the porous medium and P_0 its air entry value.

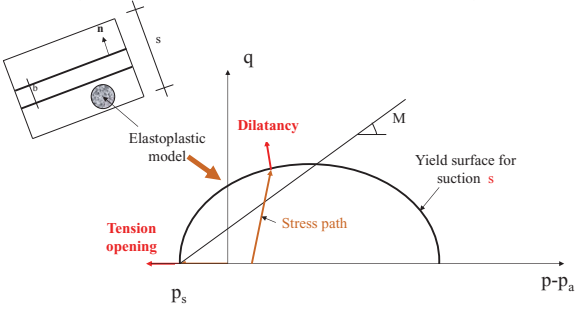

Fig. 1. Embedded fracture in a continuous element.

The effects of introducing this "embedded discontinuity" into the analysis are illustrated in Figure 2. It corresponds to an academic exercise[2]. A slope is initially created by excavating 15 m in a horizontal unsaturated stratum 45 m thick. A water table is assumed to exist at the base of the stratum. The excavation is performed in 40 days. Then a constant rainfall infiltration is applied to the exposed slope boundary. Two cases were solved: (a) constant permeability soil and (b) the development of discontinuities if tensile strains develop. Figure 2a shows the distribution of water pressure in the slope after a given infiltration time. It leads to the localization of shear strains, first at the slope toe and in subsequent times along a shearing band, which eventually leads to the slope failure.

If the shearing band results in a discontinuity of increased permeability and modified water retention, as discussed before, the calculated pore water pressure is substantially modified as shown in Figure 2b. The effect of this change is dramatic in terms of the safety of the slope. Pore pressures increase in the shear band (Fig. 2b) and the

calculated slope displacements tend to shorten the time to failure (Fig. 3) and, at the same time, they lead to a sudden type of failure if compared with the more "diffuse failure" predicted by the conventional analysis.

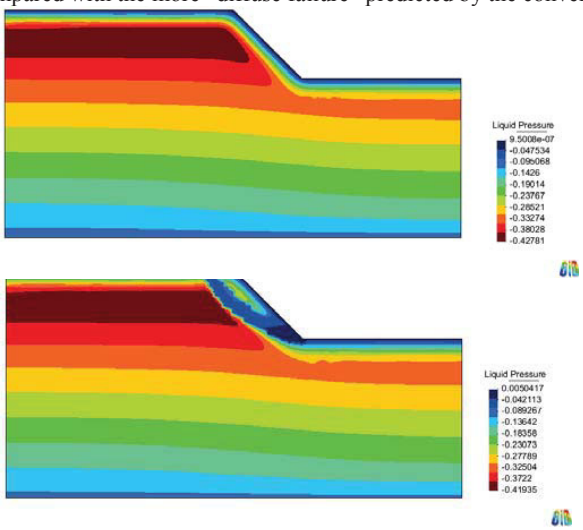

Fig. 2. Pore water pressures after rainfall infiltration. a)Uniform permeability; b) Embedded fracture.

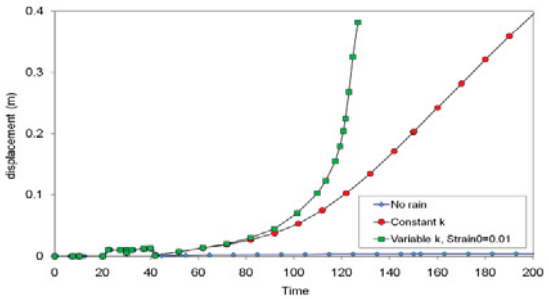

Fig. 3. Evolution of slope displacements.

2.2. Heterogeneous profiles in weathered formations

Weathered soil profiles are common in many environments and rock types[3,4]. Weathered horizons behave as a layered media of widely different permeability (and strength). The effect of such a "layering" is discussed here in connection with a case history: the instability of slopes in overconsolidated clays in the vicinity of Ancona, Italy. The slope represented in Figure 4 was selected to conduct a research study within the framework of an EU "Epoch" Project.

The slope was instrumented (the position of borings, piezometers and inclinometers is shown in Fig. 4) and rainfall was recorded in a one-year period (Fig. 5). The main emphasis of the project was to relate slope safety with rainfall, strength and hydraulic properties determined by means of tests on recovered samples. The case was described in some detail in Alonso et al. (2003)[5]. See also Agostini et al. (2013)[6]. More recently, however, the case has been reviewed and more sophisticated procedures were used to interpret the available data. The new analysis was performed with the finite element code Code_Bright[7,8].

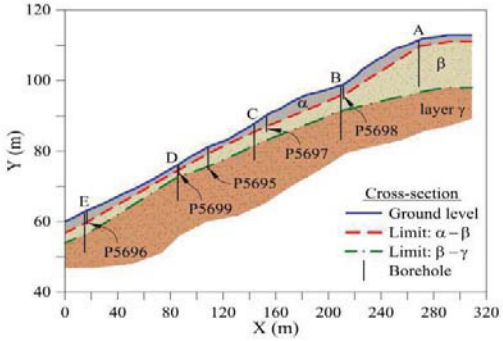

Fig. 4. Slope in Ancona clay.

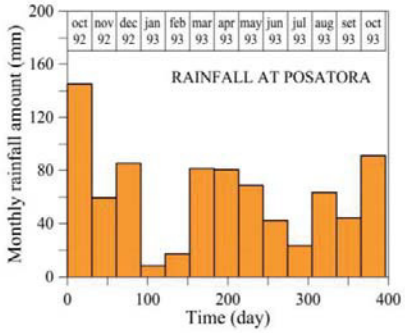

Fig. 5. Rainfall on slope in Ancona clay.

The recorded variation in pore water pressure during the year-long period of measurements was interpreted with the purpose of assigning permeability values to the three strata (α, β, γ) shown in Figure 4:

- α : Remolded brown Ancona clay rich in organic matter. CH-MH
- β : Stiff brown Ancona silty clay with sandy inclusions. CH-MH
- γ : Pliocene substratum. Blue Ancona clay

It turned out that the permeability sequence $k_\alpha = 10^{-6}$ m/s, $k_\beta = 10^{-8}$ m/s, $k_\gamma = 10^{-9}$ m/s provided the best fit between calculations and piezometer records.

The recorded rainfall intensity (Fig. 5) was applied to the slope, which was characterized by an elasto-plastic model (BBM)[9] whose parameters were approximated by interpreting suction controlled tests performed on recovered samples.

Fig. 6. Calculated plastic deviatoric strains in Ancona slope.

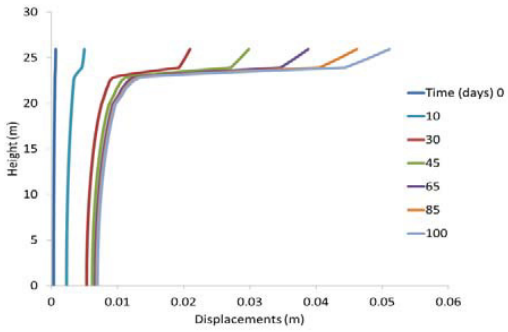

Fig. 7. Calculated displacements in Borehole "B" (see Fig. 4). Ancona slope.

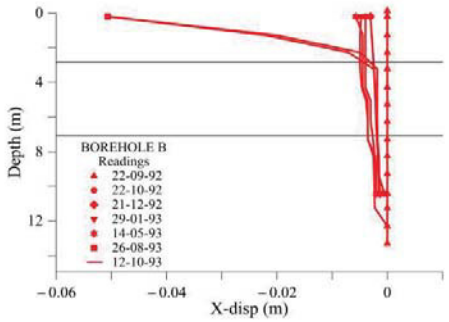

Fig. 8. Measured displacements in Borehole "B" (see Fig. 4). Ancona slope

Figure 6 shows a map of deviatoric strains at a time t = 100 days after the beginning of the analysis. Strains concentrate at the contact surface between α and β layers. This is better appreciated if horizontal displacements at the position of borehole B (see Fig. 4), along a vertical profile, are plotted as a function of time (Fig. 7). This figure may be compared with actual inclinometer records at the same position (Fig. 8). The plot shows a distinct sliding motion affecting the α layer. It develops suddenly at some intermediate time between 14/05/1993 and 26/08/1993. The reason for this instability concentrated in the upper α layer is given in Figure 9. Even if the slope is initially assumed to be in equilibrium with a deep water table (at a depth of 20 m), the accumulation of rainfall induces a progressive saturation of upper layers. However, the α layer, due to its high permeability, develops a linear increase in pore pressure from the start of infiltration. Pore pressures remain negative during a certain time, but eventually become positive and a maximum (positive) pore pressure is computed at the contact between α and β layers. Interestingly, negative pore pressures (suction) may coexist at increasing depth, making it very unlikely for a sliding surface to develop at depth.

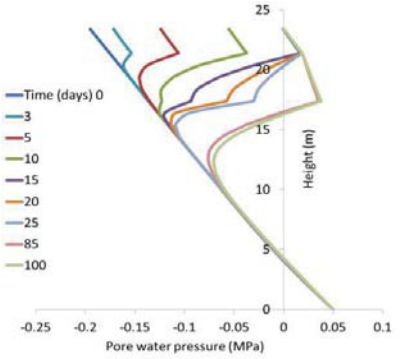

Fig. 9. Vertical profiles of calculated pore water pressure at different times. Ancona slide

3. Large deformations

3.1. Basis of MPM

The difficulties of finite element methods to deal with large deformations have prompted the development of alternative computational procedures. They are useful in landslide analysis especially when landslide velocity, acceleration and run out are of particular interest because of their direct connection with risk issues.

The methods developed may be grouped in three broad classes: (a) “true particle” methods; (b) depth integrated methods, and (c) a combination of finite element methods and Lagrangian integration points. In true particle methods (Distinct Element Methods, Discontinuous Deformation Analysis) a difficulty is to relate “contact” properties to (continuum) constitutive behavior. The role of water is also difficult to model. Depth integrated models borrow a solution methodology for viscous flow and they are useful to analyze the propagation of flow slides.

We are interested here in methods that reproduce the sliding mechanism as the original source of instability and moreover, they are capable of following the transition from static to dynamic conditions. They incorporate our current understanding of constitutive soil behavior and may also profit from the accumulated development of finite element methods. There are several variants for the Lagrangian (or “particle”, or “material points”) integration methods: SPH, PFEM, EEMLIP, MPM. We concentrate on the Material Point Method (MPM)[10] because of some of its advantages to deal with slope stability problems: a fixed computational mesh that facilitates the simulation of shear banding; the easier formulation of boundary conditions; its relatively lower computational effort compared with other methods; and its proximity to existing finite element methodologies.

The main ideas behind MPM are:

- It uses two kinds of spatial discretization to describe the porous media:
  - The material points defined over the material domain.

- The nodal mesh defined over the computational domain.

- All the information (strain, stress, velocity and pore-pressure) is carried by the material points.
- Each material point represents a portion of the domain. The mass of such subdomain is considered to be concentrated in the corresponding material point.
- The governing equations are solved at the nodes of the mesh.
- Information between material points and the mesh is mapped using conventional shape functions.

The computational cycle is illustrated in Figure 10. At the beginning of the cycle, the mass, momentum and internal forces of material points are transferred to the mesh nodes. Then the governing equilibrium equations are solved in the mesh. A momentum, Δq, is calculated by adding internal and external forces ($\boldsymbol{f}_{int}$, $\boldsymbol{f}_{ext}$) acting during a given time increment at node i and instant k:

$$\Delta \boldsymbol{q}_i^k = \left(\boldsymbol{f}_i^{int,k}, \boldsymbol{f}_i^{ext,k} \right) \Delta t \tag{4}$$

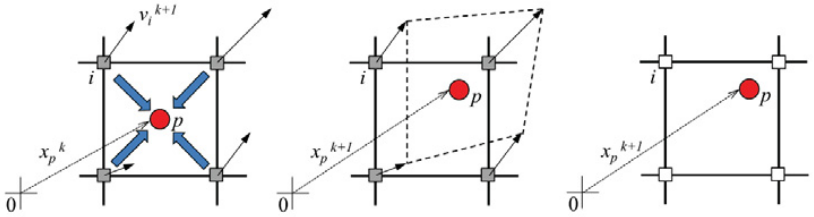

Fig. 10. Computational cycle of MPM

which allows the calculation of the velocity increment vector, v, of node i at instant k:

$$\Delta \boldsymbol{v}_i^k = \frac{\Delta \boldsymbol{v}_i^k}{m_i^k} \tag{5}$$

where m_i^k is the mass transferred from all the material points contributing to node i.

Then the updated velocity of node i at time $k + 1$ can be calculated ($\boldsymbol{v}_i^{k+1} = \boldsymbol{v}_i^k + \Delta \boldsymbol{v}_i^k$).

Knowing the velocities of all the nodes of the mesh (Fig. 10a), the velocities of each material point P, $\boldsymbol{v}_p^{k+1}$, are calculated using shape functions and then, the new position at time (k+1) is :

$$\boldsymbol{X}_p^{k+1} = \boldsymbol{X}_p^{k+1} + \boldsymbol{v}_p^{k+1} \Delta t \tag{6}$$

Displacements are then transformed into strains and stresses are computed following the selected constitutive model.

An extension of the method to deal with saturated porous media was described by Zabala & Alonso[11], Jassim et al[12] and Abe[13].

3.2. Some solved cases

Consider first the scenario described in Figure 11. A saturated slope, initially stable, is taken to critical conditions by increasing the water pressure on the lower boundary of the domain. The discretization of the domain and the imposed boundary and initial conditions are shown in Figure 12. The circle symbols indicate that the movement along the boundaries is restricted in the normal direction. The applied increase in pore pressure (40 kPa) on the lower boundary induces an upward transient water flow. The elements of the mesh are actually three-dimensional tetrahedra and material points were distributed by assigning one point per element. The mesh is refined in the area where concentrations of deformations and stresses are expected.

The soil is represented by a brittle Mohr-Coulomb model in which the effective cohesion and effective friction angle reduces as accumulated plastic deviatoric strain ($\varepsilon_{eq}^{\Delta}$) increases:

$$\Delta c' = -\left(c_p - c_r'\right)\left(1 - e^{-\eta} \varepsilon_{eq}^{\Delta}\right) \tag{7a}$$

$$\Delta\varphi' = -\left(\varphi_p - \varphi'_r\right)\left(1 - e^{-\eta\varepsilon^{\Delta}_{eq}}\right) \tag{7b}$$

Coefficient η defines the rate of loss of cohesion and friction. As the water pressure increases the shear bands evolve and coalesce in the manner indicated in Figure 13(a,b,c). The slope is still "stable" in the classical sense, when reaching the strain localization shown in Figure 14c. Immediately afterwards, the motion starts and follows the sequence shown in Figure 13(e,f,g).

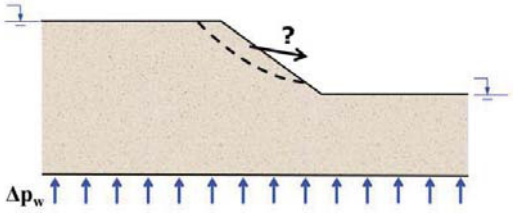

Fig. 11. A solved case by MPM. Soil properties: E = 20000 kPa; ν = 0.3; γd = 20 kN/m3; n = 0.2; k = 0.001 m/s; c' = 1 → 0 kPa; φ' = 35º → 25º

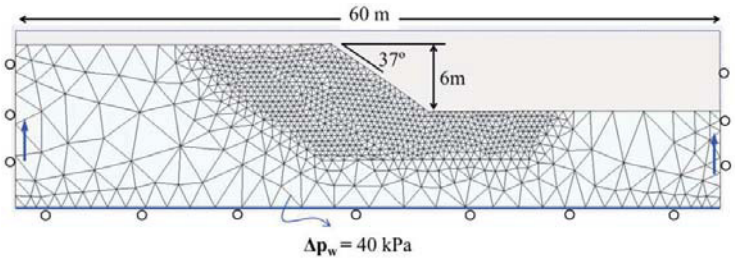

Fig. 12. MPM mesh and boundary conditions.

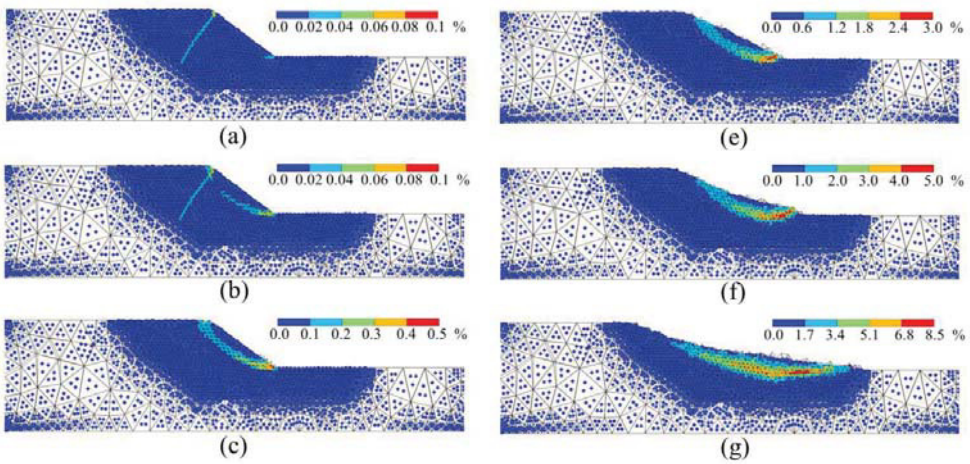

Fig. 13. (a) (b) (c) Progressive failure and shear banding; (d) (e) (f) Calculated motion of the slope. Contours of total shear strain are superimposed on plots

The calculated displacements of three points of the unstable mass located close to the failure surface are plotted as a function in time in Figure 14. The displacement increases with the height of the point above the slope foot. The upper part of the slope travels 9 m, against 3.5 m for the lower part. The maximum velocity is calculated a short

time after the initiation of the run out. Velocities also increase with the height above the base.

The example analyzed is similar to the real case of the Selborne experiment[14]. The slope was excavated in overconsolidated brittle high plasticity Gault clay and the failure was triggered by injecting water in the area ("recharge zone") shown in Figure 15a. Inclinometer readings only provide information of the very early stages of the instability because inclinometer tubes are sheared by small slope motions. This is illustrated by the displacement-time records plotted in Figure 15b.

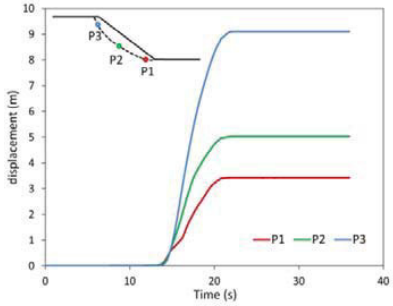

Fig. 14. Calculated displacements of three points of the moving mass

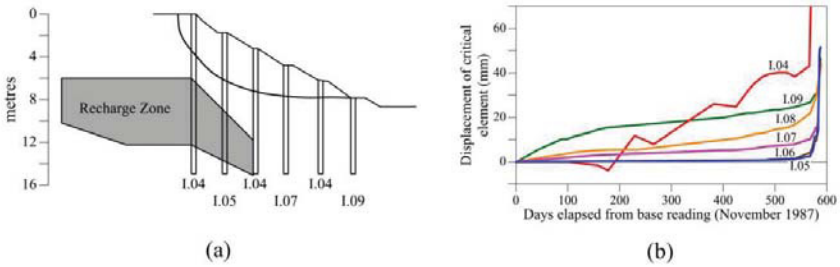

Fig. 15. Selborne failure slope experiment. a) Cross section and position of inclinometer. b) Recorded displacements in time.

A second example is the failure of Aznalcóllar rockfill dam, founded on overconsolidated marine brittle high plasticity Guadalquivir clay. The case has been described in several papers[15,16,17]. The actual failure surface could be precisely identified because of the many investigation borings performed after the failure (Fig. 16). The development of the progressive failure was reported by Zabala & Alonso[11]. Figure 17 shows the initiation of a shear band and its progression in the downstream and upstream directions until a continuous failure surface was generated. It was shown that the final shape of the failure surface, which was very similar to the actual one, could only be found by assuming an earth pressure coefficient $K_0 = 1$.

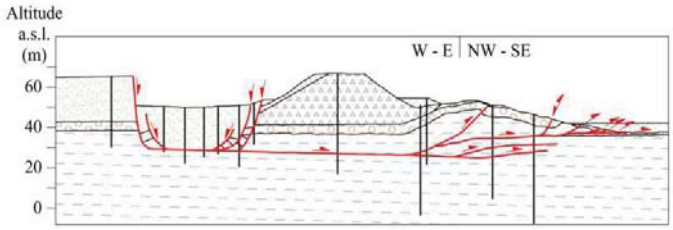

Fig. 16. Aznalcóllar dam failure

Aznalcóllar dam was built in a "downstream" manner, increasing the dam height and width, but maintaining the

position of the upstream slope. There was an interest in exploring the conditions leading to a particular geometry of the failure surface. Four cases were compared. They have been collected in Table 1.

The sensitivity analysis investigates two aspects: The characteristics of the strain softening behavior and the effect of the construction sequence. Case 1 in Table 1 describes what is believed to be the real case. In fact, according to shear tests, apparent cohesion vanished fast at the early stages of shearing. Friction was lost progressively from a peak angle of 24º to a residual value of 11º. Cases 3 and 4 in Table 1 indicate two alternatives: a constant friction angle of 17º and no cohesion and a degradation of cohesion at a constant friction angle of 17º. This friction angle was shown to lead to strict equilibrium in a conventional limit equilibrium analysis. Finally, in Case 2, the dam weight (and geometry) was applied in a single step, but the actual strength degradation was maintained.

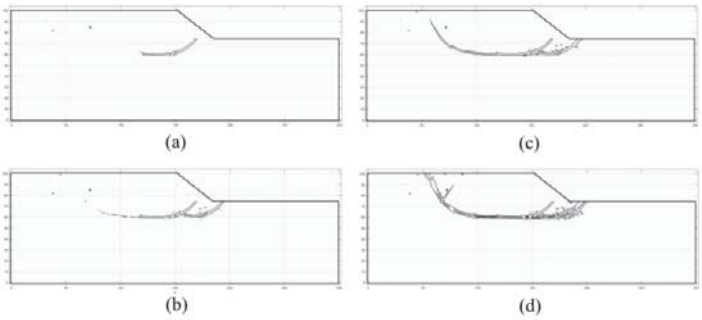

Fig. 17. Development of Aznalcóllar failure surface[11].

Table 1. Aznalcóllar dam failure. Sensitivity analysis. Cases analyzed.

Case	Effective cohesion (kPa)	Effective friction angle (º)	Construction sequence
1	$65 \rightarrow 0$	24–11	Actual staged construction
2	$65 \rightarrow 0$	24–11	Final geometry in a single step in an interval t = 7,300 days
3	0	17 (constant)	Actual staged construction
4	$65 \rightarrow 0$	17 (constant)	Actual staged construction

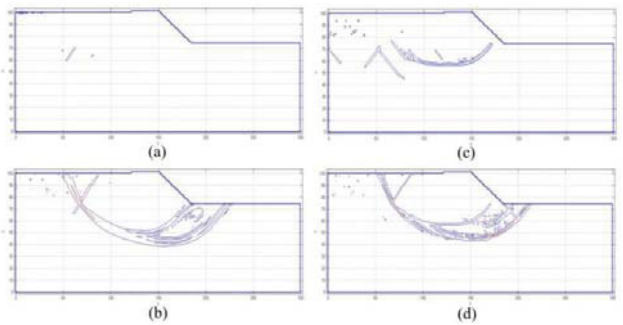

Fig. 18. Sensitivity analysis of Aznalcóllar dam. a) Case 2; b) Case 3; c) and d) Case 4. Refer to Table 1

The application of the dam (and tailings reservoir) load in a single step was far from inducing any significant yielding (Fig. 18a). A constant friction soil (no cohesion), even if the dam and its reservoir is built according to the actual construction sequence, results in a deep circular failure surface, far from the planar shape of the actual failure

surface (Fig. 18b). Case 4 introduces significant strength degradation but only in the cohesion intercept. Initially the shear bands seem to define a planar failure surface, but eventually a circular failure surface dominates the clay yielding (Figs. 18c and d).

The analysis outlined shows the complexities of failure surface development, especially in strain softening materials. Details of the strength loss and its relationship with accumulated shear straining are important. But equally significant are the geometrical details and the evolution of boundary conditions, the generation and evolution of pore water pressure and the initial stress state, which is seldom measured in practice.

4. Conclusions

The relevant role of permeability to explain the effect of rainfall on slopes is highlighted in the first part of the paper. Two aspects are discussed: the role of discontinuities and the effects of layering (or weathered horizons). Open discontinuities, either pre-existing or induced during the deformation process, result in major changes in (equivalent) permeability, which have a profound effect on the slope response against rainfall infiltration.

In soft clayey rocks and other weatherable materials, the atmospheric action leads to the development of well-defined horizons and marked changes in properties, in particular their permeability and water retention properties. It appears that failure surfaces are located at the internal boundaries defining sharp changes in permeability. Positive pore pressures may develop at these interfaces even if the soil remains unsaturated at greater depths.

In a second part, the capabilities of the Material Point Method to simulate in an integrated manner the static conditions leading to failure and the subsequent run-out are illustrated. Two examples are discussed: the instability of a slope subjected to a progressive increase in pore water pressure and a sensitivity analysis inspired in an actual failure: Aznalcóllar dam. In both cases the soil is a brittle material, typically an overconsolidated high plasticity clay. The transition from safe "static" conditions to the dynamic part of the motion does not require any "ad hoc" change in properties. It was also shown that the actual geometry of the failure surface is the consequence of many aspects: details of the strain softening behavior, the sequence of "loading" or changes in boundary conditions, the particular evolution of pore water pressures and the initial stress state. In summary, this is a complex problem.

References

1. Olivella S, Alonso EE. Gas flow through clay barriers. *Géotechnique* 2008;**58(3)**:157-176.
2. Olivella S. Geotechnical and environmental models involving unsaturated soils and rocks. In: Alonso EE, Gens A, editors. *Proceedings of the 5th International Conference on Unsaturated Soils, UNSAT2010*. Barcelona, Spain, 6-8 September 2010. London: Taylor and Francis Group; 2011.p 15-32.
3. Cafaro F, Cotecchia F. Structure degradation and changes in the mechanical behaviour of a stiff clay due to weathering. *Géotechnique* 2001;**51**:441 – 453.
4. Alonso EE, Pinyol NM. Slope stability in slightly fissured claystones and marls. Submitted to *Landslides* 2014.
5. Alonso EE, Gens A, Delahaye CH. Influence of rainfall on the deformation and stability of a slope in overconsolidated clays: a case study. *Hydrogeol J* 2003; **11**:174-192.
6. Agostini A, Tofani V, Nolesini T, Gigli G, Tanteri L, Rosi A, Cardenili S, Casagli N. A new appraisal of the Ancona landslide based on geotechnical investigations and stability modelling. *Quart J Eng Geol Hydrogeol* 2013;**47(1)**:29-43.
7. Olivella S, Gens A, Carrera J, Alonso EE. Numerical formulation for simulator (CODE_BRIGHT) for coupled analysis of saline media. *Eng Comp* 1996;**13(7)**:87-112.
8. DIT-UPC. *CODE_BRIGHT. 3-D program for thermo-hydro-mechanical analysis in geological media. User's Guide*. Barcelona: Centro Internacional de Métodos Numéricos en Ingeniería (CIMNE); 2010.
9. Alonso EE, Gens A, Josa A. A constitutive model for partially saturated soils. *Géotechnique* 1990;**40(3)**:405-430.
10. Sulsky D, Schreyer HL. Axisymmetric form of the material point method with applications to upsetting and Taylor impact problems. *Comp Meth Appl Mech Eng* 1996;**139(1-4)**:409-429.
11. Alonso EE, Zabala F. Progressive failure of Aznalcóllar dam using the material point method. *Géotechnique* 2011;**61(9)**:795-808.
12. Jassim I, Stolle D, Vermeer P. Two-phase dynamic analysis by material point method. *Int J Numer Anal Meth Geomech* 2013;**37(15)**:2502-2522.
13. Abe K, Soga K, Bandara S. Material Point Method for Coupled Hydromechanical Problems. *J Geotech Geoenviron Eng* 2014;**140(3)**:1-16.
14. Cooper MR, Bromhead EN, Petley DJ, Grant DI. The Selborne cutting stability experiment. *Géotechnique* 1998;**48(1)**:83-101.
15. Alonso EE, Gens A. Aznalcóllar dam failure. Part 1: Field observations and material properties. *Géotechnique* 2006;**56(3)**:165-183.
16. Alonso EE, Gens A. Aznalcóllar dam failure. Part 3: Dynamics of the motion. *Géotechnique* 2006;**56(3)**:203-210.
17. Gens A, Alonso EE. Aznalcóllar dam failure. Part 2: Stability conditions and failure mechanism. *Géotechnique* 2006;**56(3)**:185-201.